High Sensitivity Ge-on-Si Single-Photon Avalanche Diode Detectors

LOURDES FERRE LLIN[1], JAROSŁAW KIRDODA[1], FIONA THORBURN[2], LAURA L. HUDDLESTON[2], ZOË M. GREENER[2], KATERYNA KUZMENKO[2], PETER VINES[2], DEREK C. S. DUMAS[1], ROSS W. MILLAR[1], GERALD S. BULLER[2], AND DOUGLAS J. PAUL[1,*]

[1]James Watt School of Engineering, University of Glasgow, Rankine Building, Oakfield Avenue, Glasgow, G12 8LT, U.K.
[2]Institute of Photonics and Quantum Sciences, School of Engineering and Physical Sciences, Heriot-Watt University, Edinburgh EH14 4AS, U.K.
[*]Corresponding author: Douglas.Paul@glasgow.ac.uk

Compiled October 27, 2020

The performance of planar geometry Ge-on-Si single photon avalanche diode (SPAD) detectors of 26 μm diameter are presented. Record low dark count rates are observed, remaining less than 100 k counts per second at 6.6% excess bias and 125 K. Single-photon detection efficiencies are found to be up to 29.4%, and are shown to be temperature insensitive. These performance characteristics lead to a significantly reduced noise equivalent power (NEP) of 7.7×10^{-17} W Hz$^{-\frac{1}{2}}$ compared to prior planar devices, and represent a 2 orders of magnitude reduction in NEP compared to previous Ge-on-Si mesa devices of a comparable diameter. Low jitter values of 134 $\pm$ 10 ps are demonstrated.

http://dx.doi.org/10.1364/ao.XX.XXXXXX

Single-photon detectors are essential for a range of quantum technology applications such as quantum communications [1], quantum optics [2] and photonic quantum information processing [3] applications. They can also provide significant benefit compared to conventional p-i-n and linear avalanche photodetectors (APDs) for a range of applications including rangefinding, Light Detection And Ranging (LiDAR) [4], facial recognition and covert imaging applications. CMOS single-photon avalanche diode (SPAD) detectors [5] have been available for a number of years but are limited to operation below $\sim$1 μm wavelength, due to the absorption properties of Si. There are many significant advantages for specific applications in the short wave infrared (SWIR), which cannot be achieved using existing CMOS technology. Long distance fiber-based quantum communication systems operate predominantly at wavelengths (λ) = 1550 nm to minimize loss and require high performance SWIR single-photon detectors [1].

Furthermore, there are significant advantages in the SWIR for LiDAR and rangefinding applications. The eye-safe laser power levels increase at longer wavelengths as the photon energy decreases. For example, moving from λ = 850 nm to 1550 nm results in the ability to increase the source power by a factor of at least 20 whilst remaining inside IEC-60825-1 eye safe limits. These applications also benefit from reduced solar background at SWIR wavelengths and improved atmospheric transparency due to reduced optical scattering from water, snow, smoke, fog and dust [6]. Imaging and range-finding has been demonstrated with InGaAs/InP single-photon cameras at 1550 nm, 10 km ranges and $\leq$ 10 mW average laser power levels [4]. At this wavelength, stand-off detection and 3D imaging has been demonstrated through high levels of atmospheric obscurants [7]. Video rates depth imaging (50 frames per second) at 330 m standoff distance has been demonstrated using complex targets [8]. LiDAR has also been demonstrated with planar geometry Ge-on-Si SPADs [9] at 1450 nm [10].

For SWIR applications, the Si bandgap prevents any efficient detection of photons and therefore alternative, more expensive materials must be used. Superconducting nanowire detectors offer high-efficiency single-photon detection performance at longer wavelengths, however there is a requirement for cryogenic cooling [11]. InGaAs/InP SPADs operating on Peltier coolers at 223 K at the important telecoms 1310 nm and 1550 nm wavelengths typically have single photon detection efficiencies (SPDE) ranging from 17.5% to 34% [1, 12]. Single pixels and small imaging array Geiger mode cameras have been demonstrated. Whilst Peltier-cooled InGaAs/InP SPADs are generally lower cost than superconducting detectors, the technology is still relatively expensive compared to Si-based single-photon detectors, an especially important consideration for mass-market applications.

A potential way to produce cheap SWIR single-photon detectors is to use heterostructures on top of Si substrates that absorb photons at longer wavelengths [13]. Dual temperature growth techniques [14] have enabled growth of high quality Ge layers on Si, well above the critical thickness due to strain. Such layers have small tensile strain from the growth process, therefore providing absorption at wavelengths up to $\sim$1.6 μm at room temperature. Despite the relatively high density of misfit dislocations at the Ge/Si heterointerface and threading dislocation densities in the Ge of $\sim 10^7$ cm^{-2}, high quality p-i-n and linear avalanche photodetectors have been demonstrated [14].

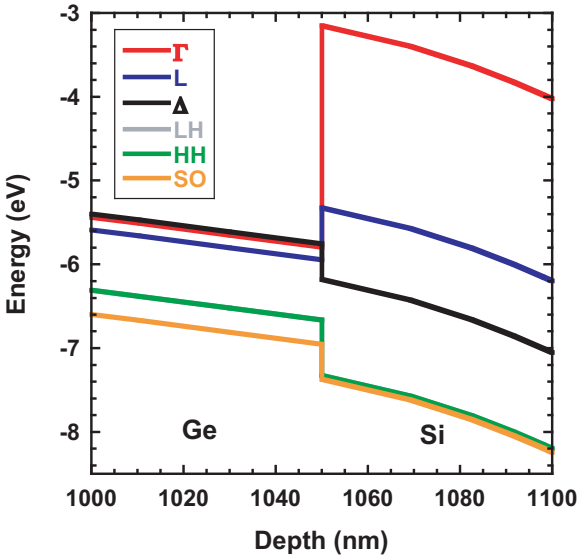

Fig. 1. A self-consistent Poisson-Schrödinger calculation of the Ge-on-Si SPAD energy bands around the Ge/Si heterointerface at 125 K and 40 V applied bias (breakdown).

Geiger mode Ge-on-Si APDs were first demonstrated by Lu et al. [15], where the devices where operated at λ = 1310 nm, with dark count rate (DCR) levels $> 3 \times 10^7$ counts per second (cps) at 180 K. We have previously demonstrated mesa etched Ge-on-Si SPADs with SPDE of 4% at λ = 1310 nm and DCR of 6 Mcps [16]. These devices also demonstrated the first single-photon detection at 1550 nm from any Si based device. More recently we have used a planar process design to improve the SPDE to 38% at λ = 1310 nm and 125 K for 100 μm diameter SPAD devices with DCRs of 2 Mcps and 310 ps jitter [9]. Similar to CMOS based SPADs [17], our previous Ge-on-Si devices [9] demonstrated lower afterpulsing than commercial InGaAs/InP SPADs, when operated under identical conditions, highlighting their potential for high repetition-rate applications. Afterpulsing is the triggering of a device due to charges released from traps that were filled from a previous avalanche [9]. This can severely limit the counting rate of the detector, which can particularly affect those applications that may use high photon count rates, such as quantum key distribution or LiDAR.

In this work we investigate the performance of planar 26 μm diameter Ge-on-Si SPADs. The observed significant reduction in DCR, whilst maintaining high detection efficiency, allows SPAD operation with a record low noise equivalent power (NEP) of 7.7×10^{-17} W Hz$^{-\frac{1}{2}}$ at a wavelength of 1310 nm and an operating temperature of 100 K. The spectral properties are identical to those presented in [9]. This step-change in performance highlights the potential for high efficiency Si foundry compatible SPAD arrays operating in the SWIR.

The devices were fabricated using 150 mm diameter n^{++} Si (001) substrates, with 1.5 μm thickness of nominally undoped Si grown epitaxially on top using an ASM Epsilon 2000E reduced pressure chemical vapor deposition (RPCVD) system. The Si foundry process follows ref. [9] with an improved planarization process. Photolithography was used to define windows for the sheet charge layers for each individual SPAD device which were implanted using B at 10 keV and activated using a 950°C anneal for 30 s. This sheet charge layer is required to mediate the electric field between the Ge absorber and the Si avalanche region (Fig. 1). The wafers were then cleaned before growing 1 μm of undoped Ge and a 50 nm p^{++}-Ge cap for the top contact. Photolithography and a fluorine inductively coupled plasma reactive ion etch (ICP-RIE) [18] were used to etch the p^{++}-Ge cap to define the top contact area. Photolithography was then used to define trenches between the SPAD devices and a fluorine ICP-RIE etched through the Ge epilayers to provide lateral electrical isolation. The device was planarized using hydrogen silsesquioxane (HSQ) and ICP-plasma enhanced chemical vapor deposition (PECVD). Si_3N_4 which was also used as an anti-reflection coating. Ti/Al was evaporated onto the backside of the wafers and annealed to form a bottom Ohmic contact to the n^{++} Si substrate. Photolithography was then used to form via holes to the p^{++} cap before Ti/Al metal was deposited to form an Ohmic contact to the top of the device.

A self-consistent Poisson-Schrödinger solution of the heterolayers was calculated using the lattice parameters, deformation potentials, energy and Varshni parameters in ref. [19]. Figure 1, shows the band-structure of a 100 nm region around the Ge/Si heterointerface, at an avalanche breakdown voltage of 40 V and 125 K. The electric field in the Si avalanche region is 2.7 times higher than the field in the Ge absorber. The photo-generated carriers are generated at the Γ-valley, but scatter to the L-valley within 100 fs [20]. The L-valley electrons in the Ge absorber are injected into the Si at an energy of 235 meV above the Δ-valley conduction band edge resulting in temperature independent SPDE. This is in contrast to InGaAs/InP SPAD detectors, where the photo-generated hole has to overcome an energy barrier of 345 meV to be injected into the avalanche region [21].

SPDE, DCR and jitter characterization of all devices were performed on the SPAD device in a cryostat with optical windows using the time-correlated single-photon counting (TCSPC) method as detailed in refs. [9, 16]. After careful power calibration, a λ = 1310 nm picosecond pulsed laser was attenuated to less than 0.01 photons per pulse, ensuring that the probability of more than 1 incident photon per pulse was statistically negligible. The SPAD devices were operated with a fixed dc voltage just below the avalanche breakdown voltage. A pulsed electrical source was used to take the device above breakdown

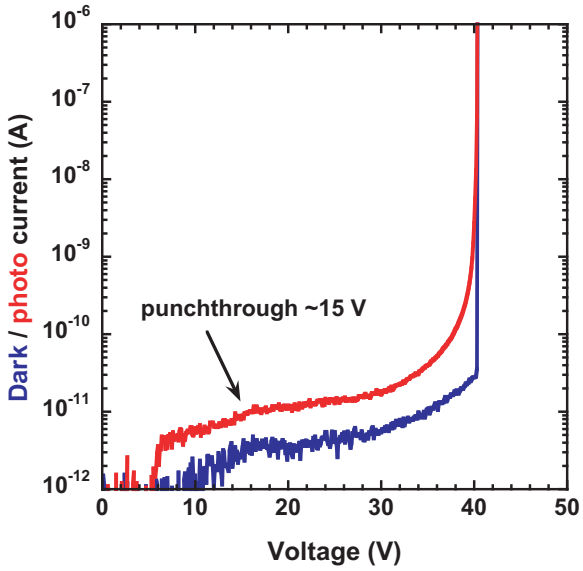

Fig. 2. The dark current (red) and photocurrent (blue) for λ = 1310 nm illumination at 125 K.

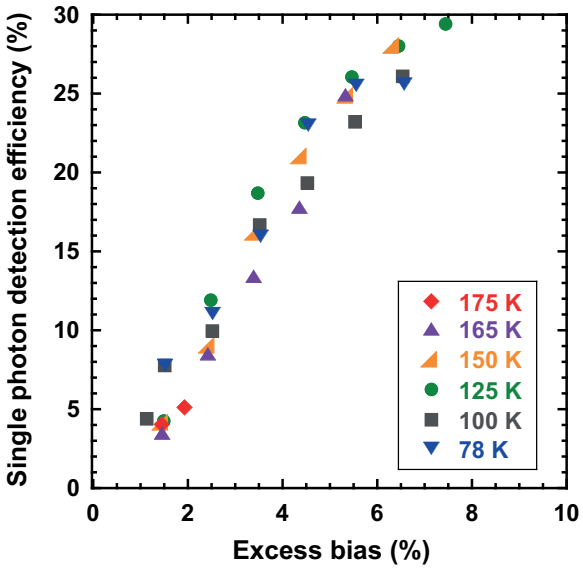

Fig. 3. The SPDE of 26 μm diameter Ge-on-Si SPADs as a function of temperature and excess bias at λ = 1310 nm.

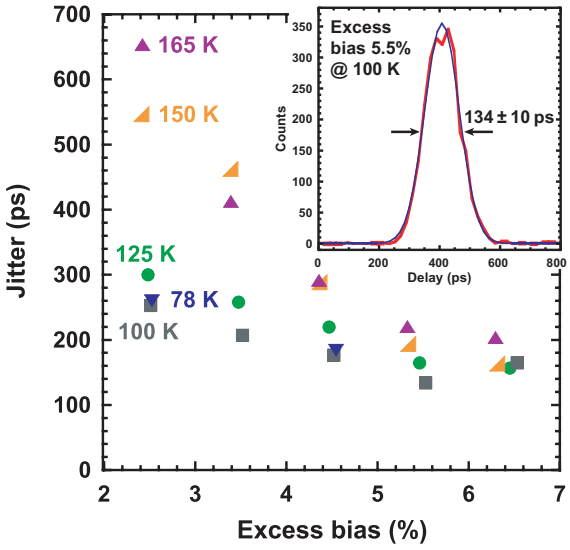

Fig. 5. The jitter of 26 μm diameter Ge-on-Si SPADs as a function of temperature and excess bias. The insert shows the timing histogram for the lowest recorded jitter (data in red, Gaussian fit in blue) obtained at 5.5% excess bias and 100 K.

for $\sim$ 50 ns, in synchronization with the incident optical pulse. This electrical pulse takes the device into Geiger mode by applying an excess bias above avalanche breakdown. The measurements were undertaken at a low repetition rate of 10 kHz (the 78 K data at 1 kHz) to provide an extremely low probability ($< 10^{-3}$) of any afterpulse effects perturbing the measurements for $\geq$ 100 K [9]. The photon counting data acquisition used for all measurements had a timing bin width of 19.5 ps. The paper presents results from an individual device but 6 devices tested demonstrated nominally identical results.

The dark current and photo-current with λ = 1310 nm illumination are presented in Fig. 2 at 125 K. The breakdown is just over 40 V at 125 K. Punch-through is visible in this measurement at $\sim$ 15 V. Figure 3 presents the SPDE and Fig. 4 the DCR

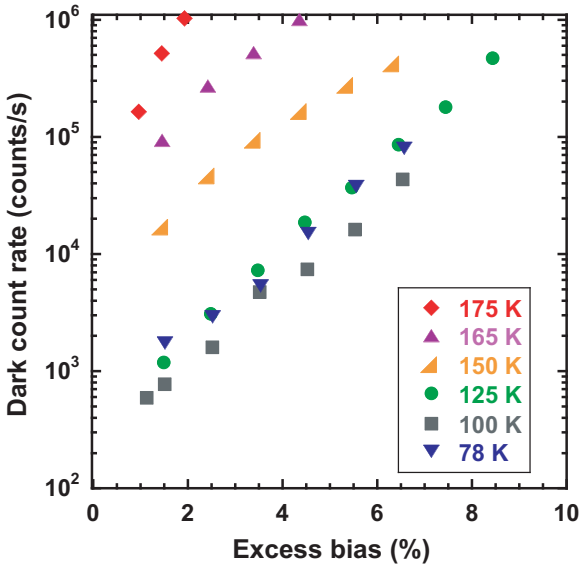

Fig. 4. The DCR of 26 μm diameter Ge-on-Si SPADs as a function of temperature and excess bias.

as function of excess bias and temperature. At 125 K, the DCR remains below 100 kcps at excess biases up to 6.6% where the SPDE reaches 28.0%. At this temperature, the maximum SPDE measured was 29.4% at the higher excess bias of 7.5%.

Previously, a 100 μm diameter device operated at 5.5% excess bias and 125 K, had a DCR of $\sim$ 2 Mcps resulting in a DCR per μm^2 of 256 cps/μm^2. This new 26 μm diameter device exhibits a DCR of $\sim$ 36.9 kcps at the same excess bias and temperature, resulting in a DCR per μm^2 of 69 cps/μm^2, realizing an improvement from the new process of a factor of $\sim$ 3.7. The DCR clearly increases with increasing temperature from 100 K to 175 K as is expected from Fermi-Dirac statistics. This is not the case for the 78 K results which have higher DCR when compared at the same excess biases to the 100 K and 125 K results. For the 78 K results, the higher DCR indicates a higher trapping of carriers at the lowest measured temperature, suggesting that these DCR measurement may include the effects of afterpulsing which becomes more evident in such low dark count devices.

As shown in Fig. 3, the SPDE is relatively constant as a function of temperature for each excess bias due to the band structure in Fig. 1 and saturates at $\sim$ 7.5% excess bias. At 175 K, the DCR becomes too high to accurately measure SPDE at all but the lowest excess biases. Whilst these results clearly indicate significantly improved sensitivity in these 26 μm diameter devices, the peak SPDE of 29.4% is less than the 38% maximum SPDE found in the 100 μm diameter devices reported previously [9]. There were indications of a non-uniform efficiency profile across the detector, and since our measurements used a spot size of $\sim$ 10 μm diameter, it is possible that we measured an averaged SPDE which is lower than the peak value.

The jitter was measured from the TCSPC histograms at 1310 nm and is demonstrated in Fig. 5 as a function of excess bias for temperatures up to 165 K. The lowest jitter (defined as the full width half maximum of the timing histogram) was 134 $\pm$ 10 ps at 100 K and increases to 204 $\pm$ 10 ps at 165 K. The minimum result at 100 K is over a factor of 2 below the lowest jitter of 310 ps reported for the 100 μm diameter planar devices [9]. In all

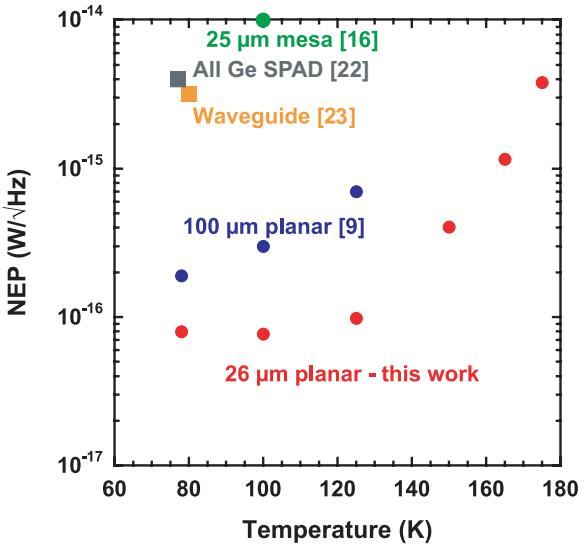

Fig. 6. NEP versus temperature from this work compared to previous reports at 1310 nm wavelength. The other results are 25 μm diameter mesa devices [16], all Ge SPADs [22], waveguides [23] and 100 μm planar devices [9].

cases, the devices were measured in a large cryostat with associated cabling. Improved packaging of these devices is likely to reduce these reported jitter values.

The NEP is an important figure of merit as it provides a valid method to compare the sensitivity of different devices at different operating temperatures and excess biases. The NEP has been calculated using

$$\mathrm{NEP} = \frac{h\nu}{\mathrm{SPDE}}\sqrt{2\mathrm{DCR}} \quad (1)$$

where h is Planck's constant and ν is the frequency. Figure 6 demonstrates the NEP as a function of temperature for the present 26 μm diameter planar devices, 100 μm diameter planar devices from [9], previous Ge-on-Si mesa devices [16], waveguide coupled Ge-on-Si SPADs [23] and all Ge SPADs [22]. The 26 μm diameter SPADs are clearly higher performance than all previous SPADs using Group IV technology at these wavelengths but have still not matched the performance of InGaAs/InP SPADs which have demonstrated 5×10^{-17} W Hz$^{-\frac{1}{2}}$ at 230 K and 1550 nm wavelength (Micro Photon Devices Srl. PDM-IR 25 μm diameter InGaAs/InP SPAD datasheet). Nevertheless, the 26 μm planar devices presented here have a NEP >2 orders of magnitude better than the comparable mesa device under similar device sizes and measurement conditions [16].

In conclusion, 26 μm diameter Ge-on-Si SPADs have been demonstrated with improved DCR, NEP and jitter compared to similar 100 μm diameter devices and all previous Group IV material devices operating in the SWIR region. Improved detector performance was observed, including SPDE of 25% with DCR of <1 Mcps at temperatures up to 165 K, with the larger DCR at higher temperatures limiting the device performance. Higher temperature operation is required for Ge-on-Si SPADs to have maintained efficiency at λ = 1550 nm from direct bandgap absorption [24]. Whilst there is a clear reduction in DCR with reduced area, further optimisation is required to reduce the DCR further if Peltier cooler operating temperatures, as required for most applications, is to be achieved.

FUNDING

UK EPSRC (EP/N003446/1, EP/ K015338/1, EP/L024020/1, EP/M01326X/1, EPN003225/1, EP/S026428/1); DSTL PhD scholarship (DSTLX-1000092774); InnovateUK (104615); UK Royal Academy of Engineering Research Fellowship Scheme (Project RF-201819-18-187).

DISCLOSURES

The authors declare no conflicts of interest.

REFERENCES

1. J. Zhang, M. A. Itzler, H. Zbinden, and J.-W. Pan, Light. Sci. Appl. **4**, e286 (2015).
2. S. Tanzilli, A. Martin, F. Kaiser, M. De Micheli, O. Alibart, and D. Ostrowsky, Laser & Photon. Rev. **6**, 115 (2012).
3. J. Wang, F. Sciarrino, A. Laing, and M. G. Thompson, Nat. Photonics (2019).
4. A. M. Pawlikowska, A. Halimi, R. A. Lamb, and G. S. Buller, Opt. Express **25**, 11919 (2017).
5. I. Gyongy, N. Calder, A. Davies, N. A. W. Dutton, R. R. Duncan, C. Rickman, P. Dalgarno, and R. K. Henderson, IEEE Transactions on Electron Devices **65**, 547 (2018).
6. G. L. Knestrick, T. H. Cosden, and J. A. Curcio, J. Opt. Soc. Am. **52**, 1010 (1962).
7. R. Tobin, A. Halimi, A. McCarthy, M. Laurenzis, F. Christnacher, and G. S. Buller, Opt. Express **27**, 4590 (2019).
8. J. Tachella, Y. Altmann, N. Mellado, A. McCarthy, R. Tobin, G. S. Buller, J.-Y. Tourneret, and S. McLaughlin, Nat. Comms. **10**, 4984 (2019).
9. P. Vines, K. Kuzmenko, J. Kirdoda, D. C. S. Dumas, M. M. Mirza, R. W. Millar, D. J. Paul, and G. S. Buller, Nat. Comms. **10**, 1086 (2019).
10. K. Kuzmenko, P. Vines, A. Halimi, R. J. Collins, A. Maccarone, A. McCarthy, Z. M. Greener, J. Kirdoda, D. C. S. Dumas, L. F. Llin, M. M. Mirza, R. W. Millar, D. J. Paul, and G. S. Buller, Opt. Express **28**, 1330 (2020).
11. R. H. Hadfield, Nat. Photonics **3**, 696 (2009).
12. L. C. Comandar, B. Fröhlich, J. F. Dynes, A. W. Sharpe, M. Lucamarini, Z. L. Yuan, R. V. Penty, and A. J. Shields, J. Appl. Phys. **117**, 083109 (2015).
13. A. Y. Loudon, P. A. Hiskett, G. S. Buller, R. T. Carline, D. C. Herbert, W. Y. Leong, and J. G. Rarity, Opt. Lett. **27**, 219 (2002).
14. J. Michel, J. Liu, and L. C. Kimerling, Nat. Photonics **4**, 527 (2010).
15. Z. Lu, Y. Kang, C. Hu, Q. Zhou, H. D. Liu, and J. C. Campbell, IEEE J. Quantum Electron. **47**, 731 (2011).
16. R. E. Warburton, G. Intermite, M. Myronov, P. Allred, D. R. Leadley, K. Gallacher, D. J. Paul, N. J. Pilgrim, L. J. M. Lever, Z. Ikonic, R. W. Kelsall, E. Huante-Ceron, A. P. Knights, and G. S. Buller, IEEE Trans. Elec. Dev. **60**, 3807 (2013).
17. D. Bronzi, S. Tisa, F. Villa, S. Bellisai, A. Tosi, and F. Zappa, IEEE Photonics Technol. Lett. **25**, 776 (2013).
18. M. M. Mirza, H. Zhou, P. Velha, X. Li, K. E. Docherty, A. Samarelli, G. Ternent, and D. J. Paul, J. Vac. Sci. Technol. B **30**, 06FF02 (2012).
19. D. J. Paul, Phys. Rev. B **77**, 155323 (2008).
20. M. P. Fischer, C. Schmidt, E. Sakat, J. Stock, A. Samarelli, J. Frigerio, M. Ortolani, D. J. Paul, G. Isella, A. Leitenstorfer, P. Biagioni, and D. Brida, Phys. Rev. Lett. **117**, 047401 (2016).
21. I. Vurgaftman, J. R. Meyer, and L. R. Ram-Mohan, J. Appl. Phys. **89**, 5815 (2001).
22. A. Tosi, A. D. Mora, F. Zappa, and S. Cova, "Ge and InGaAs/InP SPADs for single-photon detection in the near-infrared," in *Advanced Photon Counting Techniques II,* , vol. 6771 W. Becker, ed., International Society for Optics and Photonics (SPIE, 2007), pp. 133 – 144.
23. N. J. D. Martinez, M. Gehl, C. T. Derose, A. L. Starbuck, A. T. Pomerene, A. L. Lentine, D. C. Trotter, and P. S. Davids, Opt. Express **25**, 16130 (2017).
24. D. C. S. Dumas, J. Kirdoda, R. W. Millar, P. Vines, K. Kuzmenko, G. S. Buller, and D. J. Paul, Proc. SPIE **10914**, 1091424 (2019).